

Alma Mater Studiorum Università di Bologna  
Archivio istituzionale della ricerca

Experimental bond tests on masonry panels strengthened by FRP

This is the final peer-reviewed author's accepted manuscript (postprint) of the following publication:

*Published Version:*

Claudio Mazzotti, Barbara Ferracuti, Alessandro Bellini (2015). Experimental bond tests on masonry panels strengthened by FRP. COMPOSITES. PART B, ENGINEERING, 80, 223-237 [10.1016/j.compositesb.2015.05.019].

*Availability:*

This version is available at: <https://hdl.handle.net/11585/505569> since: 2021-03-16

*Published:*

DOI: <http://doi.org/10.1016/j.compositesb.2015.05.019>

*Terms of use:*

Some rights reserved. The terms and conditions for the reuse of this version of the manuscript are specified in the publishing policy. For all terms of use and more information see the publisher's website.

This item was downloaded from IRIS Università di Bologna (<https://cris.unibo.it/>).  
When citing, please refer to the published version.

(Article begins on next page)

This is the final peer-reviewed accepted manuscript of:

*Claudio Mazzotti, Barbara Ferracuti, Alessandro Bellini, **Experimental bond tests on masonry panels strengthened by FRP**, Composites Part B: Engineering, Volume 80, 2015, Pages 223-237, ISSN 1359-8368*

The final published version is available online at:

<https://doi.org/10.1016/j.compositesb.2015.05.019>

Rights / License:

The terms and conditions for the reuse of this version of the manuscript are specified in the publishing policy. For all terms of use and more information see the publisher's website.

*This item was downloaded from IRIS Università di Bologna (<https://cris.unibo.it/>)*

***When citing, please refer to the published version.***

# EXPERIMENTAL BOND TESTS ON MASONRY PANELS STRENGTHENED BY FRP

Claudio MAZZOTTI<sup>1</sup>, Barbara FERRACUTI<sup>2\*</sup>, Alessandro BELLINI<sup>3</sup>

1 Associate Professor, DICAM, University of Bologna  
Viale Risorgimento 2, 40136 Bologna, *claudio.mazzotti@unibo.it*

2 Assistant Professor, DICAM, University of Bologna  
Viale Risorgimento 2, 40136 Bologna, *barbara.ferracuti@unibo.it\**

3 Researcher of the Centre for applied research - Buildings and Construction (CIRI-EC)  
University of Bologna, Via del Lazzaretto 15/5, 40136 Bologna, *alessandro.bellini5@unibo.it*

\*Corresponding author

## Abstract

The results of an experimental campaign on bond between Glass Fiber Reinforced Polymer (GFRP) sheets and single clay brick or masonry panel is presented. Four different types of clay bricks (new and ancient) are considered, where the difference between bricks is not only due to their mechanical properties but also to their surface texture. Another focus point of the experimental campaign is the effect of mortar joints on the GFRP-masonry panel bond. Moreover, the effects of different surface preparation on the debonding load were investigated, concerning both bricks and masonry panels. A total number of 38 specimens was tested and results in terms of debonding force, strain along the GFRP and failure modes are here reported. The experimental results were also compared to design formula proposed by the new version of Italian Guidelines. Furthermore, in order to numerically describe the bond behaviour of the specimens tested, non-linear interface laws were calibrated starting from the debonding load and the measured strains along the GFRP for various loading levels.

**Keywords:** A. Glass fibres; B. Debonding; D. Mechanical testing; Masonry.

# 1. Introduction

A great number of existing masonry structures are currently undergoing a severe process of structural strengthening in order to extend their service life and improve their seismic capability. Since masonry buildings are a large part of the existing European building heritage, the problem is very remarkable and needs to be addressed properly in order to assure the required level of structural safety.

Among the existing strengthening techniques, one of the most promising and capable consists of using Fiber Reinforced Polymers (FRP) sheets bonded to masonry structural elements [1][2][3]. They are very effective for confining masonry columns [4], for strengthening masonry arches [5], vaults and masonry walls [6-7] against horizontal forces, typically produced by seismic events. In most cases, the failure type of these FRP-strengthened elements is an early debonding of the reinforcement from the masonry substrate, without reaching the ultimate strength of the FRP material; usually, at the failure process is associated the removal of a thin layer of substrate.

Many experimental results on bond between brick and FRP reinforcement are actually available in the literature [8-15], while only few experimental studies [16-19] can be found concerning bond between FRP sheets and masonry panels, even if this is the real application. Recently, also the FRP sheets inclination with respect the longitudinal axis of the masonry panels is considered as one of the parameters playing an important role in the bond behaviour [20]. At present the only available design formulas for the evaluation of debonding load are based on results of numerous bond tests performed on single brick or on plain natural stone [21-22]. Therefore it is not proved that these formulas could be extended to the real case of masonry walls, made of bricks/stones and mortar joints, since it is still not definitely assessed how and to which extent this type of bond could be affected by the presence of mortar joints

among artificial bricks or among natural stones. On the contrary, from the numerical point of view the effect of mortar joints is accurately addressed by many authors [19][23-26].

Another important aspect that can affect the bond strength is the surface preparation. In fact, in many practical applications with the purpose of reducing the irregularity of masonry surface a finishing is applied on it before gluing the FRP sheets. This finishing could completely change the mechanical behaviour of bond, shifting the debonding layer from the FRP-brick interface to FRP-finishing interface depending on many factors, i.e. the quality of the surface finishing, the compatibility between the epoxy resin and the finishing, the time interval between the applications of the finishing itself and the epoxy resin.

In this framework, the main goal of the present research is the experimental investigation of:

i) bond behaviour between Glass Fibers Reinforced Polymer (GFRP) sheets and brick masonry panels compared to the bond behaviour between FRP sheets and single brick, ii) the effect of the brick type on bond strength, iii) the effect of different surface finishing, realized by using two different types of mortar, with the purpose of regularizing the masonry surface.

In particular, a total number of 38 specimens made of four different clay brick types and with three surface finishing were tested. Sixteen specimens were prepared without the application of any surface finishing, six specimens were finished with the application of a natural hydraulic lime based mortar (low mechanical performance) and sixteen specimens were finished with a two-component polymer modified cementitious based mortar (high mechanical performance).

Failure modes, measurement of bond strength and longitudinal strain distributions along the GFRP bonded part were observed and discussed, in order to draw general conclusions or useful recommendations. The measured debonding loads were also compared with predictive formulas proposed in Italian Guidelines [27].

Difference in the bond behavior between the single clay brick and the masonry panel was accurately described by a specific analysis of the debonding process, based on the evolution of the strain profile. By post-processing the experimental results, observations about effective bond lengths and maximum shear stress were made, distinguishing the bond behaviour into two fundamental phases: until the onset of debonding a sort of “static bond” can be observed while during the debonding phase a “dynamic shifting bond” governs the process. In order to numerically model the bond mechanism two different non-linear interface laws, one for each phase, were proposed.

## **2. Materials and experimental setup**

### **2.1 Material Mechanical Properties and Specimen Preparation**

In the present experimental campaign, three main aspects were investigated, concerning the bond behaviour of GFRP sheets: the effect of various types of clay bricks with different mechanical properties and surface textures, the interface behaviour of GFRP sheets bonded to a single brick or to a masonry panel (with presence of mortar joints between the bricks) and the role of the surface finishing made using two different types of mortar.

All the specimens were prepared using four different types of clay bricks: the first three types (1-3) were new elements produced with standard industrial processes (Figure 1a-c), whereas type 4 was an old (already used) brick coming from demolition of existing masonry building (Figure 1d). The mechanical characterization of bricks was done by means of compression tests and three-points bending tests [28-29]; corresponding results are reported, together with mean dimensions of bricks, in Table 1. As expected, brick type 4 shows a larger variability of dimensions and mechanical properties, probably due to the process of extraction from demolished building.

Masonry panels tested in the experimental campaign were made of 6 clay bricks separated by

1 mortar joints. Their thickness is about 10 mm for all the masonry specimens, except for type  
2 4, where the irregular shape of bricks required a thickness of about 15 mm. In order to  
3 manufacture the masonry specimens, a commercial mortar was used based on natural  
4 hydraulic lime and selected aggregates with a maximum diameter of 4 mm. Its compressive  
5 and tensile strength were, respectively, 4.13 MPa and 1.05 MPa. Each masonry panel was cut  
6 in two parts so to obtain two specimens from each element, as shown in Figure 2, with mean  
7 geometrical dimensions reported in Table 2.  
8

9 The name and number of bricks and masonry specimens tested is shown in Table 3. The first  
10 letter indicates single brick (B) or masonry (M) specimens; the following number is related to  
11 the type of brick used (1-4); the second letter identifies the type of surface finishing: A =  
12 specimens with naked bricks, B = specimens finished with a natural hydraulic lime mortar, C  
13 = specimens finished with a two-component polymer modified cementitious mortar; the last  
14 number identifies different tested specimens with the same properties and components.  
15

16 The mortar used for surface finishing identified as B is the same used to manufacture the  
17 mortar joints in all masonry specimens. Thickness and mechanical properties of the two types  
18 of mortar are reported in Table 4.  
19

20 All the specimens were reinforced by applying unidirectional GFRP sheets with dry thickness  
21  $t_f = 0.172$  mm and width  $b_f = 50$  mm. According to technical data provided by the producer,  
22 the sheet has a density of  $430 \text{ g/m}^2$  and a minimum tensile strength of 2300 MPa. Measured  
23 mean value of elastic modulus is 123767 MPa instead of 76000 MPa suggested by the  
24 producer. Sheets were glued to clay bricks and to masonry panels by using a two –  
25 components epoxy resin; its tensile strength and elastic modulus were 30 MPa and 4500 MPa,  
26 respectively (according to producer data). No primer before bonding was used. Curing period  
27 of all specimens was at least 7 days prior to testing.  
28  
29  
30  
31  
32  
33  
34  
35  
36  
37  
38  
39  
40  
41  
42  
43  
44  
45  
46  
47  
48  
49  
50  
51  
52  
53  
54  
55  
56  
57  
58  
59  
60  
61  
62  
63  
64  
65

In the present experimental investigation, for all the specimens the GFRP bonded length BL, shown in Figure 3, was equal to 200 mm. GFRP sheet bonded length starts 30 mm ( $L_1$ ) far from the front side of brick specimens and 100 mm ( $L_1$ ) far from the front side of masonry panel specimens. In this way, according to [30], the interface behavior should not be affected by boundary effects and it is then more representative of the material behavior far from cracked sections (FRP end debonding). With the purpose of having comparable tests on specimens made both of single brick or masonry panel, the FRP sheet width and the support (brick or masonry panel) width were chosen in such a way to obtain for all the tests a ratio between the widths of about 0.4.

## 2.2 The Experimental Setup and Instrumentations

The experimental set-ups adopted for bond tests on bricks and masonry panels are shown in Figure 4a,b, respectively. Both types of specimens were placed on a rigid support completed by front and rear steel reaction elements, positioned to prevent horizontal and vertical displacements; front reaction element left a vertical free surface  $d$  of the specimen of about 20 mm height (depending on the brick height  $h$  or for masonry panel on the brick dimension  $B$ ); the system devoted to the vertical constraining was constituted by four steel C-shaped clamping elements, which were placed on both sides of the specimen. The free extremity of the GFRP sheet was mechanically clamped within a two steel plate system, where the traction force was applied by means of a mechanical actuator. Tests were then performed by controlling the stroke displacement of sheet free end and imposing a rate of 0.3 mm/min.

Concerning the instrumentations, a load cell was used to measure the applied traction force during tests and a series of seven strain gauges was placed along the GFRP sheet centreline in order to measure longitudinal strains. Spacing between strain gauges are reported in Figure 3. For both bricks and masonry panels, the same strain gauge positions were adopted.



### 3. Results of bond tests

#### 3.1 Global response: Debonding load and failure mode

##### A – Specimens without surface preparation

In Figure 5, debonding force results obtained from the 16 tests performed on bricks and masonry panels without surface preparation (A) are shown. Eight of them are GFRP-brick bond tests (B1A-B4A) and eight are GFRP-masonry panels bond tests (M1A-M4A). Comparing the results of tests performed on the same brick type, it is observed that in most cases (brick Types 1, 2 and 4) the measured debonding forces are larger for masonry panels, with an increase between 10 and 20% with respect to GFRP-single brick tests. These differences are mainly due to two factors: (i) the presence of the mortar joints in the masonry panels, (ii) the difference in the surfaces of brick sides, where the FRP is glued.

Regarding the first aspect, the presence of the mortar joints makes the debonded surface more irregular, with the thickness of the detached mortar larger than that of the detached brick. This suggests that the mortar joints generated a higher mechanical interlock compared to the clay bricks only.

The second factor is related to the different surface roughness of brick sides; in fact, in the single brick test the FRP is glued to the surface is with mean dimensions 250x125 mm (upper side); while, for masonry panel the FRP is bonded to brick side with mean dimensions 250x50 mm (lateral side). These two brick sides have different mechanical properties and surface porosities, due to the different position during the brick producing and firing process. In general, the surface porosities/roughness have an important role on the bond strength [31], because the greater is the surface porosity, the greater will be the capacity of the adhesive to penetrate in the brick substrate making the fracture energy, necessary for the debonding, increase. In Figure 6, where pictures of the two different brick sides for brick Type 2 and 3 are reported, it is possible to observe that for type 2 the surface (lateral side) used to glue the

FRP in masonry panels is rougher than the surface (upper side) used to glue the FRP in single brick specimens. Therefore, a stronger adhesion between FRP reinforcement and masonry panels is expected with respect to the brick case. On the contrary, in the case of brick type 3 the surface roughness of the two sides are the opposite, which explains why for the specific case of brick type 3, differently to the other three brick types, the debonding load is higher in the tests on brick specimens with respect to the measured load in tests on masonry panels. Another factor explaining different debonding load results between brick specimens and masonry panels is the anisotropic behaviour of brick, as already observed in [32] making compression tests on cylindrical cores extracted from the upper surface and from the lateral surface.

Considering only the results from GFRP-single brick bond tests (B1A-B4A), as expected, the debonding force is strictly related to the brick compressive and tensile strengths (Table 1) and, in particular, increases with growing values of the product of these mechanical parameters. This confirms the theoretical approach to evaluate the debonding load which can be found in the CNR Guidelines [27], that proposed an analytical formula similar to that adopted when considering the concrete substrate:

$$F_{Th} = b_f \sqrt{2E_f k_b k_{Gm} \cdot \sqrt{f_{bc} f_{bt}}} , \quad (1)$$

where  $k_b$  is the width factor taking the three-dimensional effect of the FRP reinforcement into account and  $k_{Gm}$  is the mean value of the calibration coefficient. An update of this calibration coefficient is proposed in [21-22] with a lower value of  $k_{Gm}$  for clay brick ( $k_{Gm} = 0.05$ ). This calibration coefficient was defined starting from an extended database containing only bond tests on FRP-single brick specimens and by adopting in Eqn. (1) the simplified expression  $f_{bt}=1/10 f_{bc}$ , since the measured tensile strength was not available in most part of tests found in the literature. Moreover, in most of the experimental studies, the FRP Young's modulus was not measured and the nominal value given by the producers was adopted. Even if in the

present experimental campaign the bricks mechanical properties were measured with proper tests, according to the assumption adopted during the calibration of the design formula eq.(1), the theoretical loads were calculated for the present specimens using the simplified expression of tensile strength. Nevertheless, comparison between experimental and predicted mean values, reported in Table 5, shows that in the present case predictions strongly overestimate the experimental findings. However, introducing the declared FRP Young's modulus instead of the measured one, the error is significantly reduced.

In the authors' opinion this result remarks the importance of measuring the mechanical properties of bricks and FRP reinforcement adopted in experimental campaigns, because they can be very different with respect to the declared nominal values and can affect the reliability of prediction formula.

Concluding the discussion about the formula providing the debonding load in masonry structure strengthened by FRP, it is important to remark that until now no design formula is provided yet able to take specifically into account the presence of the mortar joints, therefore no distinction in the prediction of debonding load for single brick and masonry specimens can be made.

In all the tests performed on bricks and masonry panels without surface finishing, the failure mode was cohesive debonding failure, caused by shearing and detachment of a thin layer of clay brick, 1-2 mm thick; some examples of the brick surface (in brick tests) after debonding are reported in Figure 7. Thickness of clay brick attached to the adhesive was uniform under the whole FRP sheet. In only three cases, over sixteen specimens, detachment of a prism with triangular cross-section (see Figure 7b) occurred due to unbalanced tensile stresses localized to the front of the specimen. The boundary effect was observed when using the bricks types 1, 2 and 3 but not in a systematic way. This debonding failure mode occurs only in the test on the single brick, where the unbonded brick length to the front of the specimen was shorter (30

mm) with respect to the case of masonry panel (100 mm). Only in one case (specimen B4A1) failure occurred due to GFRP sheet rupture, at a load of 7.4 kN. The type of failure mode for each specimen is also summarized in Table 5.

Figure 8 shows the failure mode of all types of masonry panels without surface finishing (A). In this case, it is possible to observe that both clay brick and mortar joints are attached to the GFRP sheet. As mentioned before, the thickness of the attached mortar joints is usually greater than that of clay brick layers, creating a sort of global saw-tooth profile which is able to generate a greater mechanical interlock, compared to the single clay brick case.

#### B - Surface preparation with lime mortar

The second aspect investigated in the present experimental campaign is the effect of masonry surface finishing on the debonding load. In Figure 9a, values of debonding forces obtained from the 6 tests performed on specimens (bricks and panels) with surface preparation identified as “B” (low performance finishing) are reported: type 3 and type 4 bricks only are used in these tests. In particular, only one test has been performed for each type of single brick and the results are shown as mean values.

Application of a mortar based on natural hydraulic lime (NHL) to the surface of the specimens, single bricks or masonry panels, causes a significant reduction (more than 30%) in the maximum value of force registered during the test, compared to the specimens without surface preparation. Therefore, adopting a low quality mortar just for the purpose of regularizing the masonry surface leads to an ineffective adhesion of the strengthening. Figures 10 a, b shows the debonding failure modes for B3B1 and M3B1 specimens: in both cases the crisis occurs within the NHL mortar used to finish the surface.

### C - Surface preparation with polymer modified cementitious mortar

The second adopted finishing mortar, a two-component polymer modified cementitious mortar (C), is really effective increasing the debonding force of specimens (Figure 9b). Increments in terms of debonding force with respect to the case without finishing are reported in Table 6, where it is observed a large increment of about 60-80 % for the brick types 1 and 2, with low brick's strength and an increase of about 15-20% for the brick types with higher strengths.

Similarly to the case of specimens without surface finishing the debonding forces obtained by masonry specimens generally show higher values with respect to the case of single bricks. In particular, the percentage of the increment of debonding force depends on the quality of the brick type. This finishing type is particularly effective in the case of bricks with poor quality.

The bond failure modes for brick and masonry specimens finished with two-component polymer modified cementitious mortar are shown in Figures 11 and 12, respectively. Figures 11a-b show two different failure modes observed in the present experimental campaign. In the first one (B2C1 specimen) the debonding surface is located within the brick (DB failure mode). Instead in the second one (specimen B4C1) the debonding occurred with the removal of a finishing mortar layer (DBF failure mode). Also for masonry panels the two different failure modes (DB and DBF) were observed (see Figure 12a,b). In specimen M1C1 (Figure 12a), the crisis is fully located within the masonry prism, just below the surface finishing, instead for specimen M3C1 the debonding is located within the finishing layer. In other cases the failure mode was intermediate between the two failure modes above described (DB and DBF).

For all the specimens, the failure modes are summarized in Table 6 and it is observed that in most cases failure occurs because of debonding at the finishing mortar-epoxy interface. Nevertheless, presence of polymer-modified mortar (C) strongly increased the debonding load

with respect to the case without surface preparation (A) and made such a force less sensitive to the bricks mechanical properties. Finally, the observed failure modes at the mortar-epoxy interface are due to the fact that the strengthening system (epoxy+GFRP) was applied when the mortar below was already cured. This result shows the importance of applying the epoxy on the mortar still chemically active, like suggested in some international Guidelines [27]; in this case, an even greater bond strength can be expected and the failure would probably shift within the masonry.

Table 6 reports also the comparison between the debonding force obtained by tests and by an empirical formula, proposed by [27], taking the beneficial effects of a finishing layer into account. In all cases, the predictive law strongly overestimates the debonding force, this suggests that future improvements to this formulation are needed.

Even if the number of tests is not large enough to draw final conclusions, the obtained results, both in terms of failure mode and of bond strength, suggest that performing bond tests on bricks only provides for results “on the safe side” with respect to those obtained from corresponding masonry panels.

### 3.2 Global response: Force-elongation curves

Force–elongation curves obtained from the experimental tests, performed on specimens with and without surface finishing, are compared in Figure 13; for reason of space, results from one specimen only for each type of brick and masonry panel are reported.

The FRP elongation reported in diagrams was obtained by a consolidated integration process, starting from the measured strains along the GFRP sheet (further details can be found in [33]).

Elongation is intended here as the length increase of the FRP bonded part, which is coincident with the slip between FRP and masonry evaluated at the initial bonded cross-section (on the front of the specimen) if the latter is considered as rigid.

Figures 13a-f show that in all cases the force-slip curve is characterized by an almost linear initial branch up to the onset of debonding, irrespective of the type of brick, presence of mortar joints or surface finishing. After that point, the debonding process is characterized by a variable force, due to the brittleness of the debonding failure mode. The shape of this part of the curves depends from the specific type of specimen considered.

If specimens with naked surfaces (Figure 13a,b) are taken into account, within each type of specimens the slope of the first branch is always very similar, irrespective of the type of brick.

For single brick tests (Figure 13a), the peak load was usually reached at the very beginning of the debonding phase and was followed by a softening branch. Masonry panels showed a different debonding curve (Figure 13b): after first debonding (at the end of the almost linear branch) a small force reduction is observed followed by a remarkable further force increase and a final discontinuous saw-tooth shaped line. This original behavior can be explained by considering the different bond between FRP-brick and FRP-mortar joint, with the latter probably weaker than the former. Accordingly, when the maximum transmissible force from the first bonded brick of the panel is attained, there is a discontinuity of the curve meaning that the bond has been suddenly transferred to the next brick without effectively interesting the mortar layer. As a confirmation, the first peak can be found at a lower force level, with respect to the following, since the GFRP sheet is effectively transmitting force almost only to the first bonded brick (Figure 8b, *partial anchorage* on a part of the brick thickness), which is shorter than the entire brick thickness; following peaks correspond to higher force levels and are self-similar since now the GFRP is effectively bonded to the whole thickness of following bricks (Figure 8b, *total anchorage*). This typical behaviour in bond tests performed on masonry panels, observed also by [17][18], is not clearly visible in the curves of M1A and M2A specimens, which had the poorest mechanical properties of the bricks. This behaviour

will be explained better after analysing the evolution of the local response at the deformation level in section 4.

Force-elongation curves for brick and masonry panels finished with hydraulic lime mortar (B, low mechanical properties) are shown in Figure 13*c-d*. Irrespective of the type of brick considered, the maximum load registered during these tests was considerably lower than those measured from previous bond tests; this is due to the low properties of the mortar used for the finishing of the surface, which can be very effective to smooth the surface and reduce the peeling effect, but has not adequate mechanical properties for shear strength. Also the ultimate elongation at failure is sensibly reduced with respect to previous cases, increasing the brittleness of the system. Finally, the deformability of the lime mortar reduces also the initial stiffness of the reinforcement in both cases of single brick and masonry panel.

Figure 13*e,f* show the force-elongation curves obtained for brick specimens and masonry panels, respectively, finished with two-component polymer modified cementitious mortar (C); the high values of maximum load registered confirms that this surface preparation is really effective to increase the bond strength: the positive effect of surface regularization, in fact, is due to the high mechanical characteristics of the adopted mortar. Beneficial effects are particularly apparent when considering substrates with reduced mechanical properties (bricks type 1 and 2). A further consequence of the finishing layer application is the smoothing of the saw-tooth shaped portion of the force-elongation curves, corresponding to the debonding phase (Figure 13*f* vs 13*b*). Presence of the finishing mortar, in fact, reduces the discontinuity occurring when the effective bonded portion jumps through the weak mortar joints.

### 3.3 Local Response: Strain distribution

During the tests, the evolution of the GFRP longitudinal deformations along the centreline of the specimens were recorded and are shown in Figures 14 and 15 as a function of the



corresponding position, respectively for specimens without surface finishing (A) and with finishing mortar type C. Every curve corresponds to a given load level (up to the onset of debonding) or to a given axial elongation (during the debonding phase), which are reported on each Figure. The deformations corresponding to the first bonded cross-section ( $z = 0$  mm) were not measured directly but the following theoretical value  $\varepsilon = F/EA$ , depending on the applied force  $F$  and on the axial stiffness of the reinforcement  $EA$ , was used. From a qualitative viewpoint, the strain distributions are similar to those typical of FRP-concrete interfaces [30], both for bricks and masonry panels: an initial (at low levels of applied load) exponential decay type distribution is observed followed, for higher loads, by the S-shaped strain distribution proving the on-going debonding. In fact, strains tend to be almost constant along the GFRP sheet close to loaded end, due to the shifting of debonding phenomenon along the bonded length; where debonding has not yet occurred, an exponential decay behaviour can still be observed. Finally, in many cases a quite stable debonding process was observed because of sufficiently long bonded lengths considered.

Figures 14 shows the strain distribution along the sheets for specimens without surface preparation (A); both results from bricks (Figures 14*a,c,e,g*) and masonry panels (Figure 14*b,d,f,h*) tests are reported. In particular, positions of bricks and mortar joints along the specimens are depicted under each graph corresponding to masonry panels (Figure 14*b,d,f,h*). In all cases, before the onset of debonding the strain distributions go very rapidly to zero, meaning that the portion of substrate involved in the shear force transfer is very limited. This portion represents the initial effective bonded length,  $EBL_1$ , of the reinforcement. However, during the debonding process, two phases with two types of strain distributions and two different EBLs are observed: i) beginning of debonding, where the portion of substrate effectively involved in the force transfer is limited and similar to those before debonding ( $EBL_1 = 40\text{-}70$  mm for single brick without finishing); ii) during the debonding, where a

much larger portion of substrate is involved in the force transfer, almost losing the S-shaped strain distribution ( $EBL_2 = 65\text{-}90$  mm for single brick without finishing). The corresponding results are reported in Table 7. Given the uncertainties due to the discrete knowledge of strains (only in the strain gauges positions), the EBL is estimated in a qualitatively manner.

Considering the masonry panels, the  $EBL_{S1}$  are significantly smaller than those of single bricks because the first part of bond length is constituted only by a part of the thickness of the first brick (see also Figure 8b *partial anchorage*). This means that before the beginning of debonding the transfer region is formed only by that first part of the brick and no significant amount of load is transfer to the second brick. Moreover, it is possible to observe that for M3 and M4 the  $EBL_1$  seems to be longer than the others but it is only due to the fact that in this two cases the thickness of the bricks is greater, therefore the anchorage length on the first brick is longer and so the  $EBL_1$ . After the onset of debonding the length involved in the force transfer systematically increases and  $EBL_2$  turns out to be comparable to that one observed in the case of single brick, because now a longer bond length is available (about center distance between two mortar joints 80 mm).

The strain profiles corresponding to specimens finished with cementitious mortar C are shown in Figure 15a-h: both bricks and masonry panels made with all the four types of brick were considered. From a qualitative standpoint, profiles are similar to previous ones (Figure 14), confirming that even with a finishing layer the debonding process is still similar to that without it. The main difference being which material remains attached to FRP reinforcement. Comparing the strain profile obtained by bricks and those obtained by masonry panels with finishing C, no significant differences are observed, since in both cases the finishing mortar layer reduces the effect of the type of substrate. As for the effective bond length (EBL), introduction of this finishing layer seems to have no changed significantly it for bricks (about  $EBL_1 = 50\text{-}70$  mm and  $EBL_2 = 70\text{-}90$  mm). On the contrary, for masonry panels the finishing

reduces the effect of the presence of mortar joints changing significantly the initial transfer region which increases from 30 mm up to 70 mm.

In conclusion, the EBL is significantly different if it is evaluated considering the beginning of debonding or during the debonding. For single brick in the first phase EBL is shorter and variable from 40 to 70 mm, while in the second phase it is longer and varies from 65 to 90 mm.

Instead, for masonry specimens it seems that the EBL is only defined by the distance between two mortar joints and no advantage in terms of load increment is obtained by elongating the anchorage length. On the contrary using effective surface finishing the EBL is not governed anymore by the positions of the mortar joints and higher values of load can be reached.

#### **4. Remarks on results from Masonry Panel tests**

The analysis of deformations is helpful not only for the previous definition of the effective bond length, but also in order to explain the different global behaviour showed by the masonry specimens with respect to single bricks, where for the first ones a discontinuous saw-tooth shaped line in force-elongation curve is observed. In Figure 16a, as an example, the F-d curve for specimens M4A is reported, where four assigned points are marked and their corresponding strain distributions are shown in Figure 16b. The first point, A, refers to the first peak load and, as shown by the corresponding strain distribution, represents the onset of debonding, which started from the first brick, where the FRP was glued only on a portion of the brick thickness (see Figure 16c). After point A, a significant reduction of load is observed until point B is reached and, as shown by the corresponding strain profile, the transfer area is shifted from the first brick, where the measured strains is quite constant, to the second one (curve B). Now the transfer length, corresponding to an entire brick thickness, is longer and the load could further increase until the peak point C, corresponding to the maximum load,

reached thanks to the bond between FRP sheet and the second brick (strain distribution  $C$  in Figure 16b). Following point  $D$  represents the full debonding of the FRP from the second brick and the shifting of the transfer region on the third and last brick. Therefore, the shape of the global force-elongation curve with discontinuous saw-tooth is directly related to the evolution of the strain distribution in some specific steps of loading phase. In particular, at any crossing of mortar joints by the maximum shear stress corresponds a force drop.

## 5. Local Interface Laws

Starting from the strain profiles recorded along the GFRP sheets for various loading steps, it is possible to calibrate non-linear interface laws able to describe the bond behavior of the specimens tested. To this purpose, different approaches are available. The most sophisticated ones are based on inverse analyses and they were already applied for the similar problem of defining the FRP-concrete interface law starting from experimental data and making use of numerical model (for further details see [34]).

In the present paper a more simple calibration technique has been performed. By post-processing the experimental results in terms of strain along the FRP sheet, the shear stress and the corresponding slip for all phases of the test can be obtained. In fact, according to [33], considering an elastic behaviour for the composite, average value of shear stress between two subsequent strain gauges can be written as a function of the difference of measured strains (process of derivation). In order to define the slip distribution along the FRP sheet, the following assumptions are made: perfect bonding (no slip) between reinforcement and substrate at last strain gauge position; 2) deformation of substrate is negligible with respect to FRP counterpart 3) linear variation of strains in FRP sheet between two subsequent strain gauges. Then, integration of strain profile gives the slip at a general abscissa  $z$ . The  $n-1$

couples of average shear stress –slip values ( $\hat{\tau}_{i+1/2}$ ,  $\hat{s}_{i+1/2}$ ) are calculated for each couple of strain gauges for all recorded steps of all tests.

As a starting point for some considerations, the results of the described procedure are reported in Figures 17a, b for a brick specimen without surface finishing (B3A) and with surface finishing type C (B2C), respectively. In both cases, the shear stress - slip curve corresponding to the first couple of strain-gauges (close to the side where force is applied) is stiffer and with a higher value of maximum shear stress (which usually led to a larger fracture energy) with respect to curves corresponding to the following couples of strain gauges. This interface behaviour is observed for almost all the specimens. The mechanical explanation of what observed is that to initiate FRP debonding, higher shear stress and energy release (area under the  $\tau$ - $s$  curve) values have to be reached, with respect to those characterizing the debonding propagation along the reinforcement. This is similar to what happens in fracture mechanics in terms of crack initiation and propagation [35-36] and can also explain why in the measured force-elongation curves of bricks specimens, after the peak value, a systematic softening branch is observed (since the debonding force is strictly related to the interface fracture energy). As a consequence of this approach, two different local interface laws were considered and identified from each test. The adopted curve for the calibration of the laws was proposed for concrete-FRP interface in [33], according to the expression:

$$\tau(s_p) = \tau_{\max} \frac{s_p}{\bar{s}} \frac{n}{(n-1) + (s_p / \bar{s})^n} \quad (3)$$

where  $\tau_{\max}$  is the shear strength,  $\bar{s}$  is the slip at peak and  $n$  is a parameter mainly governs the softening branch.

By least square minimization between theoretical and experimental shear stress–slip data the three unknown parameters of the eq. (3) are determined. For example, in case of specimen B2C, the first interface law was calibrated (Figure 18a) using only data obtained by the first

couple of strain gauge (0-1), which is useful to describe the behaviour of the first short part (10-20 mm) of the FRP bonded area; parameters characterizing the curve are:  $\tau_{\max}=5.89$  MPa,  $\bar{s}=0.048$  mm,  $n=3.86$ . Introducing these parameters in eq. (3) and by integration in closed form, the area under the interface law can be calculated in exact form and represents the fracture energy  $G_f=0.536$  N/mm. The second curve, related to the interface behaviour of the central and rear portions of the specimen, was calibrated (Figure 18b) making use of data obtained by all other couples of strain gauges; parameters characterizing the curve are:  $\tau_{\max}=3.43$  MPa,  $\bar{s}=0.076$  mm,  $n=4.14$ . Also in this case the fracture energy  $G_f=0.453$  N/mm was computed resulting smaller than the previous case, as expected, meaning that energy required to activate first debonding is greater than that necessary to make the debonding propagate along the bonded length. Similar results were also obtained for all others specimens tested but they are not reported here for reasons of space. Therefore, in the numerical modelling the authors suggest to take the observed phenomenon into account by introducing two different interface laws for describing the mechanical behaviour of the two zones of the bonded lengths.

Detailed knowledge of the interface behaviour allows to perform an accurate numerical analysis, where between the FRP reinforcement and the masonry substrate can be placed a cluster of zero-thickness interface elements [37, 38] characterized by the analytical laws calibrated as described.

## 6. Conclusions

The experimental campaign presented was focused on the investigation of three main aspects:

a) the effect of the brick type on bond strength, b) the comparison, in terms of bond behaviour, between brick and masonry specimens strengthened with the same FRP

reinforcement, c) the effect of different surface preparations (made using two different types of mortar). All the specimens were reinforced with the same type of GFRP sheet.

As for the effect of the brick type, tests on strengthened single bricks confirmed that bond strength is strongly related to the brick mechanical properties and the assumption that tensile strength is about 10% of compressive strength is often too rough and both properties should be measured.

When comparing bond capacity of strengthened single bricks and corresponding masonry panels without any surface finishing, an increase of about 10 to 20% was systematically recorded in the latter case with respect to the former. Since in the two types of tests (on bricks or masonry panels) FRP reinforcement was bonded to two different surfaces of bricks (upper side or lateral side), particular care has to be devoted in verifying that they have similar roughness; if this is not the case, even opposite results could be found. Indeed, not only the influence of mortar joints is important but also the surface roughness is paramount.

Even though all existing mortars are certainly effective in smoothing the surface of the masonry substrate, only the application of a suitable mortar with adequate mechanical properties (usually a cementitious polymer modified mortar) would increase the FRP bond strength. Moreover, effectiveness of this type of finishing seems to be larger with a weaker substrate. The application of weak mortars, on the contrary, could even cause a reduction on the maximum force.

Analysis of longitudinal strain profiles, recorded along the FRP reinforcement during the debonding process of all types of specimens, permitted to draw conclusions about the effective bond length. In particular, it is observed that for masonry specimens without surface finishing the effective bond length depends only on the geometrical distance between two mortar joints. Instead, if a high quality finishing is applied the effective bond length can be increased until about 90 mm (in this experimental campaign).

1  
2  
3  
4  
5  
6  
7  
8  
9  
10  
11  
12  
13  
14  
15  
16  
17  
18  
19  
20  
21  
22  
23  
24  
25  
26  
27  
28  
29  
30  
31  
32  
33  
34  
35  
36  
37  
38  
39  
40  
41  
42  
43  
44  
45  
46  
47  
48  
49  
50  
51  
52  
53  
54  
55  
56  
57  
58  
59  
60  
61  
62  
63  
64  
65

Finally, a detailed analysis of interface behavior observed in different positions along the FRP bonded part (in single brick tests) showed that the first portion of it, where the debonding starts, is usually characterized by a stronger shear capability with respect to the second part of the bonded length, leading to a softening branch in the force-elongation diagram. Nevertheless, this aspect needs further investigation in order to be properly clarified.

## 7. Acknowledgements

The authors would like to thank the Sika Italia S.p.A. for providing GFRP sheets and adhesives for the specimens. The financial support of (Italian) Department of Civil Protection (ReLUIIS 2014-2016 Grant – Task 5.2) is gratefully acknowledged.

## 8. References

- [1] Shrive N.G. (2006). The use of fibre reinforced polymers to improve seismic resistance of masonry. *Construction and Building Materials*, 20: 269-277.
- [2] Casareto M., Oliveri A., Romelli A. (2002). Strengthening of Masonry: Opportunities and Challenges in the Use of Composites. M. S. thesis, University of Genoa and University of Missouri-Rolla, Genoa and Rolla, Mo.
- [3] Lignola, G. P., Ceroni, F., Balsamo, A., Prota, A. and Manfredi, G. 2012. Externally Bonded Masonry Structures. *Wiley Encyclopedia of Composites*. 1–11.
- [4] Faella, C., Martinelli, E., Paciello, S., Camorani, G., Aiello, M.A., Micelli, F., Nigro, E. Masonry columns confined by composite materials: Experimental investigation. *Composites: Part B* 42 (2011) 692–704.
- [5] Cancelliere I., Imbimbo M., Sacco E. (2010). Experimental tests and numerical modeling of reinforced masonry arches, *Engineering Structures*, 32: 776-792.
- [6] Tan K.H., Patoary M.K.H. (2004). Strengthening of masonry walls against out-of plane loads using fiber-reinforced polymer reinforcement. *Journal of Composites for Construction*, 8(1): 79-87.



- [7] Vasconcelos G., Lourenço P.B. (2009). In-plane experimental behavior of stone masonry walls under cyclic loading. *J. Struct. Eng.*, 135(10): 1269-1277.
- [8] Camli U.S., Binici B. (2007). Strenght of carbon fiber reinforced polymers bonded to concrete and masonry. *Construction and Building Materials*, 21: 1431-1446.
- [9] Aiello M.A., Sciolti S.M. (2006). Bond analysis of masonry structures strengthened with CFRP sheets. *Construction and Building Materials*, 20: 90-100.
- [10] Capozucca R. (2010). Experimental FRP/SRP - historic masonry delamination. *Composite Structures*, 92: 891-903.
- [11] Cosenza E., Manfredi G., Occhiuzzi A., Pecce M.R. (2000). Toward the investigation of the interface behavior between tuff masonry and FRP fabrics. *Mechanics of masonry structures strengthened with FRP materials*, Libreria Cortina, Padova, Italy.
- [12] Grande E., Imbimbo M., Sacco E. (2011). Bond behaviour of CFRP laminates glued on clay bricks: Experimental and numerical study. *Composites: Part B*, 42: 330-340.
- [13] Garbin E., Panizza M., Valluzzi M.R. (2010). Experimental assessment of bond behavior of fibre-reinforced polymers on brick masonry. *Struct. Eng. Int.*, 20(4): 392-399.
- [14] Ghiassi B., Xavier J., Oliveira D. V., Lourenço P. B. (2013). Application of digital image correlation in investigating the bond between FRP and masonry. *Composite Structures*, 106: 340-349.
- [15] Valluzzi M.R., Oliveira D.V. , Caratelli A., Castori G., Corradi M., de Felice G., Garbin E., Garcia D., Garmendia L., Grande E., Ianniruberto U., Kwiecień A., Leone M., Lignola G. P., Lourenço P. B., Malena M., Micelli F., Panizza, M., Papanicolaou C. G., Prota A., Sacco E., Triantafillou T. C., Viskovic A., Zajac B., Zuccarino G. (2012). Round robin test for composite-to-brick shear bond characterization. *Materials and Structures*; 45; 1761-1791.
- [16] Oliveira D.V., Basilio I., Lourenço P.B. (2011). Experimental Bond Behavior of FRP Sheets Glued on Brick Masonry. *Journal of Composites for Construction*, 15(1): 32-41.
- [17] Carrara P., Ferretti D., Freddi F. (2013). Debonding behavior of ancient masonry elements strengthened with CFRP sheets. *Composites: Part B*, 45: 800-810.

- [18] Carloni C., Subramaniam K.V. (2012). FRP-Masonry Debonding: Numerical and Experimental Study of the Role of Mortar Joints. *Journal of Composites for Construction* 2012.16: 581-589.
- [19] Capozucca R. (2013). Effects of mortar layers in the delamination of GFRP bonded to historic masonry. *Composites Part B: Engineering*, 44: 639-649.
- [20] Mazzotti C., Ferracuti B., Bellini A., (2015). Experimental study on masonry panels strengthened by GFRP: the role of inclination between mortar joints and GFRP sheets, *Key Engineering Materials*, 624: 559-566, doi: 10.4028/www.scientific.net/KEM.624.559.
- [21] Ceroni F., Ferracuti B., Pecce M., Savoia M. (2014). Assessment of a bond strength model for FRP reinforcement externally bonded over masonry blocks. *Composites Part B: Engineering*, 61: 147-161.
- [22] Ceroni F., Ferracuti B., Pecce M., Savoia M. (2014). Erratum and addendum to "Assessment of a bond strength model for FRP reinforcement eternally bonded over masonry blocks, Composite part B: Engineering 61 (2014): 147-161". Submitted to *Composites Part B: Engineering*.
- [23] Ghiassi B., Oliveira D.V., Lourenço P.B., Marcari G. (2013). Numerical study of the role of mortar joints in the bond behavior of FRP-strengthened masonry. *Composites Part B: Engineering*, 46: 21-30.
- [24] Fedele R., Milani G. (2012). Assessment of bonding stresses between FRP sheets and masonry pillars during delamination tests. *Composites: Part B*, 43: 1999-2011.
- [25] Grande E., Imbimbo M., Sacco E. (2011). Simple model for bond behaviour of masonry elements strengthened with FRP. *Journal of Composites for Construction*, 15(3): 354-363.
- [26] Grande E., Imbimbo M., Sacco E. (2013). Modeling and numerical analysis of the bond behavior of masonry elements strengthened with SRP/SRG. *Composites Part B*, 55: 128-138.
- [27] CNR DT 200/R1 (2012). Guide for the Design and Construction of Externally Bonded FRP Systems for Strengthening Existing Structures, Advisory Committee on Technical Recommendation for Construction of National Research council, Rome, Italy.

- [28] UNI EN 772-1 (2002). Methods of test for masonry units – Determination of compressive strength.
- [29] UNI EN 772-16 (2005). Methods of test for masonry units – Part 16: Determination of dimensions.
- [30] Mazzotti C., Savoia M., Ferracuti B. (2009). A new single-shear setup for stable debonding of FRP-concrete joints. *Construction and Building Materials*, 23: 1529-1537.
- [31] Iovinella I., Prota, A., Mazzotti C. (2013). Influence of surface roughness on the bond of FRP laminates to concrete. *Construction and Building Materials*, 40: 533-542.
- [32] Mazzotti C., Sassoni E., Bellini A., Ferracuti B., Franzoni E. (2015). Strengthening of masonry elements by FRP: Influence of brick mechanical and microstructural properties, *Key Engineering Materials*, 624 (2015): 330-337.  
doi:10.4028/www.scientific.net/KEM.624.330.
- [33] Ferracuti B., Savoia M., Mazzotti C. (2007). Interface law for FRP-concrete delamination. *Composites Structures*, 80: 523-531.
- [34] Savoia, M., Ferracuti, B., Vincenzi, L. (2009). Inverse analysis for the calibration of FRP - Concrete interface law. *Advances in Structural Engineering* 12(5): 613 – 625, doi: 10.1260/136943309789867845.
- [35] Bažant Z.P. (2002). Concrete fracture models: testing and practice. *Eng Fract Mech*, 69(2): 165–205.
- [36] Xu S., Zhang X. (2008). Determination of fracture parameters for crack propagation in concrete using an energy approach. *Eng Fract Mech*, 75: 4292-4308.
- [37] Mazzotti C., Murgu F. (2014). Numerical modelling and experimental verification of GFRP-masonry interface behavior: bond evolution and role of the mortar layers. Submitted for publication in *Composites Part B*.
- [38] Ceroni F., de Felice G., Grande E., Malena M., Mazzotti C., Murgu F., Sacco E. and Valluzzi M. R. (2014). Analytical and numerical modeling of composite-to-brick bond. *Materials and Structures*, doi: 10.1617/s11527-014-0382-8 (in press).

Table 1. Types of clay bricks investigated in the experimental campaign: mean mechanical and geometrical properties.

Clay Brick Types	L Mean (mm)	B Mean (mm)	h Mean (mm)	Mean $f_{bc}$ (MPa)	Mean $f_{bt}$ (MPa)
Type 1	250	120	55	16.304	3.680
Type 2	250	120	55	18.233	5.907
Type 3	240	110	60	32.901	7.144
Type 4	300	127	50	29.186	9.705

Table 2. Masonry panels: geometrical properties.

Masonry panel specimens	H (mm)	L/2 (mm)
M1	380	125
M2	380	125
M3	410	120
M4	395	150

Table 3. Name and total number of the specimens tested during the experimental campaign.

Clay Brick Types	No surface preparation (A)		Surface finished with mortar (B)		Surface finished with mortar (C)	
	Clay Brick Specimens	Masonry Specimens	Clay Brick Specimens	Masonry Specimens	Clay Brick Specimens	Masonry Specimens
Type 1	B1A1 B1A2	M1A1 M1A2	-	-	B1C1 B1C2	M1C1 M1C2
Type 2	B2A1 B2A2	M2A1 M2A2	-	-	B2C1 B2C2	M2C1 M2C2
Type 3	B3A1 B3A2	M3A1 M3A2	B3B1 -	M3B1 M3B2	B3C1 B3C2	M3C1 M3C2
Type 4	B4A1 B4A2	M4A1 M4A2	B4B1 -	M4B1 M4B2	B4C1 B4C2	M4C1 M4C2
number of specimens	8	8	2	4	8	8
Total	38					

Table 4. Mortar used for surface preparation: thickness and mechanical properties.

Mortar finishing	Thickness (mm)	Mean $f_{mc}$ (MPa)	Mean $f_{mt}$ (MPa)
for brick Type 3-4 (B)	4	4.13	1.05
for brick Type 1-3 (C)	1	35*	10*
for brick Type 4 (C)	2	35*	10*

\* Data provided by the producer

Table 5. Failure modes, experimental debonding loads and theoretical debonding loads according to [21-22].

Specimen name	Failure mode	$F_{exp}$ (kN)	$F_{theor}$ (kN) $E_f meas.$	Error (%)	$F_{theor}$ (kN) $E_f decl.$	Error (%)
B1A1	DB-be	4.472	6.087	37	4.770	7
B1A2	DB	4.440				
M1A1	DB	5.339	6.115	24	4.792	-3
M1A2	DB	4.503				
B2A1	DB-be	6.340	6.437	14	5.044	-11
B2A2	DB	5.003				
M2A1	DB	6.802	6.467	0	5.067	-22
M2A2	DB	6.191				
B3A1	DB	7.356	8.559	19	6.707	-7
B3A2	DB-be	7.082				
M3A1	DB	6.522	8.647	37	6.776	7
M3A2	DB	6.130				
B4A1	SR	7.380	8.196	22	6.422	-4
B4A2	DB	6.055				
M4A1	DB	7.995	8.335	7	6.531	-16
M4A2	DB	7.548				

DB = debonding failure

DB-be = debonding failure with boundary effect on the front side

SR = GFRP sheet rupture

Table 6. Failure modes, experimental debonding loads, increments respect to the case without finishing and theoretical debonding loads according to [21-22].

Specimen name	Failure mode	$F_{exp}$ (kN)	Increment respect A [%]	$F_{theor}$ (kN)
B1C1	DBF	7.957	63	8.114
B1C2	DB	6.549		
M1C1	DB	8.918	85	8.152
M1C2	DB	9.265		
B2C1	DB	5.879	8	8.580
B2C2	DB	6.382		
M2C1	DBF	10.179	69	8.621
M2C2	SR	11.729		
B3C1	DBF-be	8.378	19	11.404
B3C2	DBF-be	8.760		
M3C1	DBF	7.765	24	11.526
M3C2	DBF	7.941		
B4C1	DBF	8.037	15	13.353
B4C2	DBF	7.377		
M4C1	DBF	9.201	16	13.595
M4C2	DBF	8.871		

DB = debonding failure

DB-be = debonding failure with boundary effect on the front side

DBF = debonding failure at the finishing level for at least 50% of the glued surface

SR = GFRP sheet rupture

Table 7. Estimation of Effective Bond Length for brick and masonry specimens with and without finishing.

	Without finishing (A)		With finishing (C)	
Brick Type	EBL <sub>1</sub> (mm)	EBL <sub>2</sub> (mm)	EBL <sub>1</sub> (mm)	EBL <sub>2</sub> (mm)
B1	70	88	50	76
B2	65	85	55	78
B3	73	90	72	85
B4	40	65	55	86
M1	25	70	78	98
M2	40	82	43	73
M3	45	70	62	80
M4	44	80	70	65

EBL1 = Effective Bond Length beginning of debonding

EBL2 = Effective Bond Length during debonding

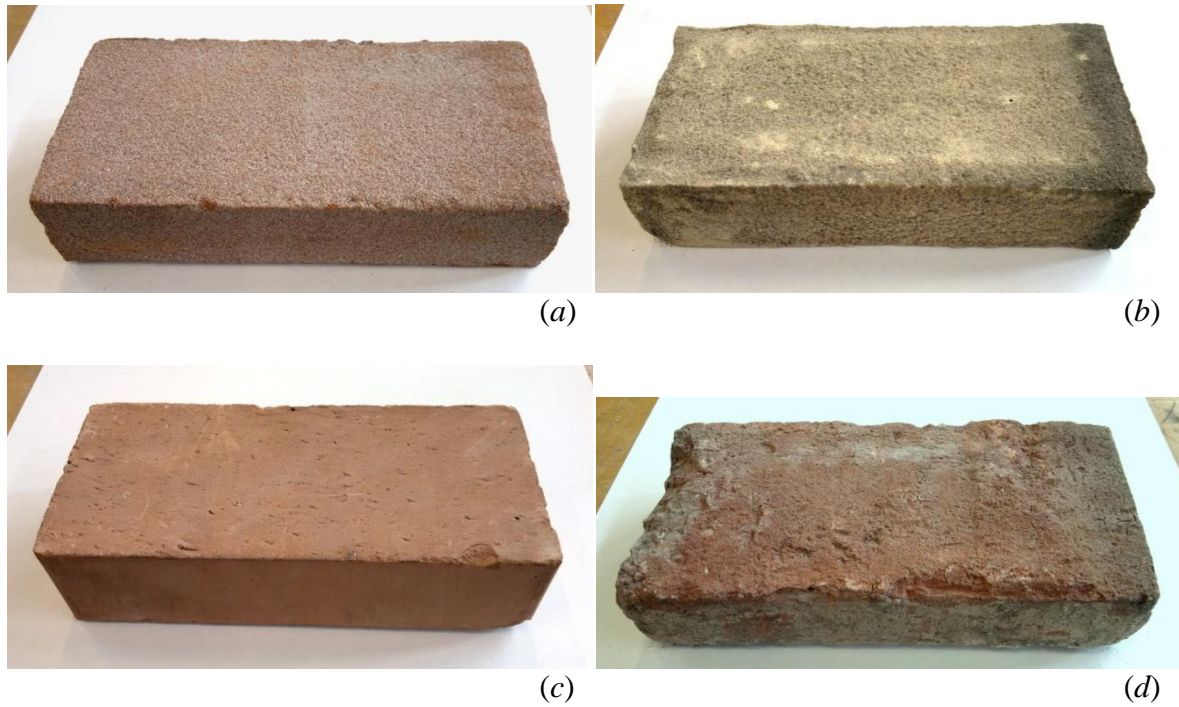


Figure 1. Types of brick used in the experimental campaign: (a) Type 1; (b) Type 2; (c) Type 3; (d) Type 4.



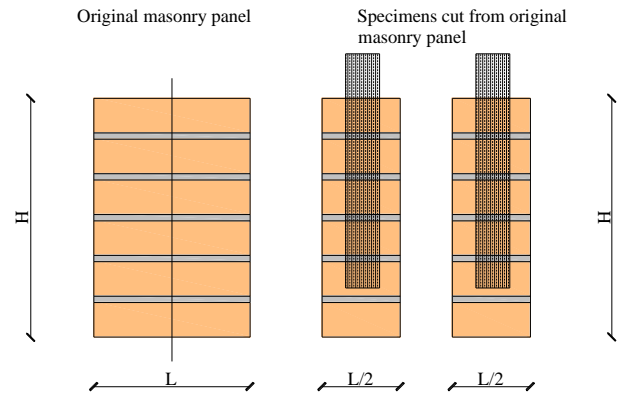


Figure 2. Geometry of masonry panel and its cutting in two parts.

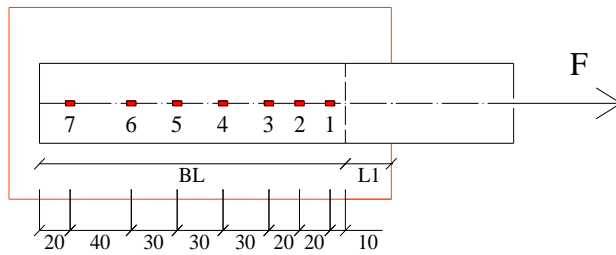


Figure 3. Instruments: Strain gauges.

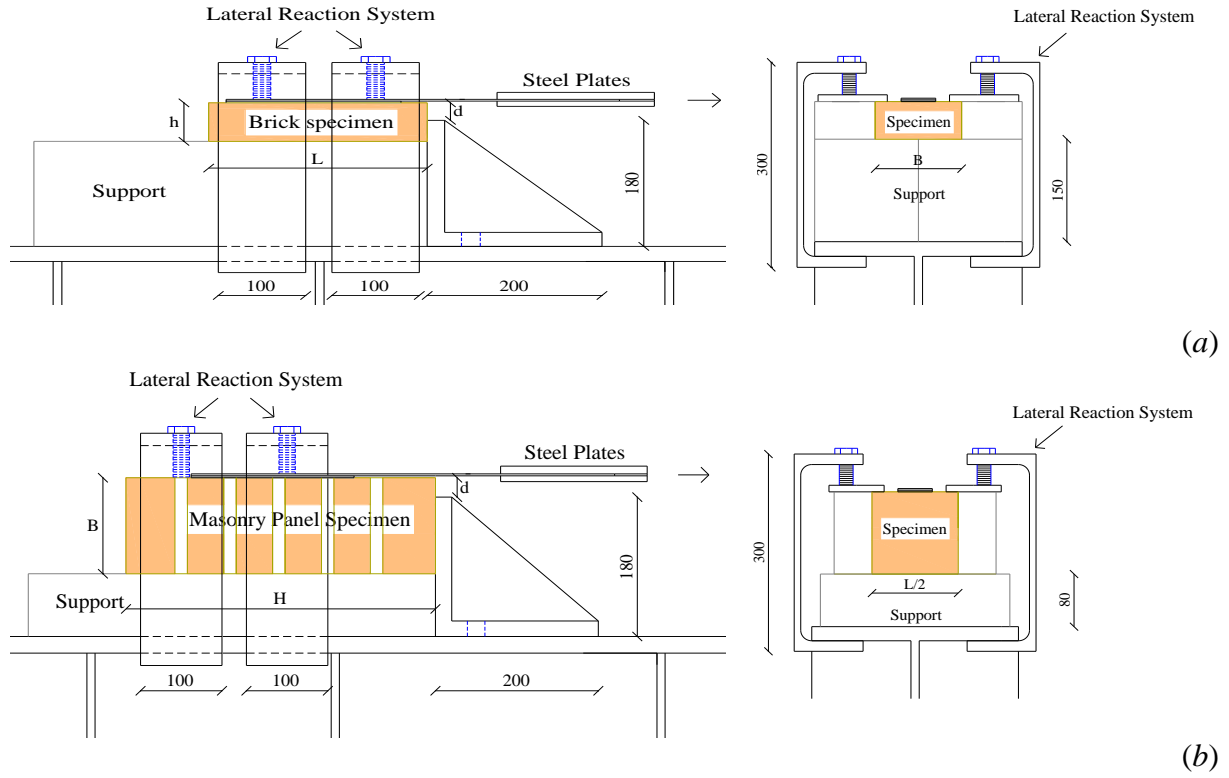


Figure 4. Experimental Setup: (a) Brick Specimen; (b) Masonry Panel Specimen.

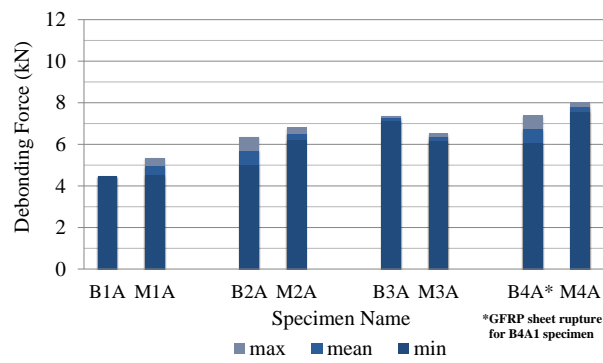


Figure 5. Maximum, minimum and mean values of debonding force obtained by the 4 different clay bricks (B1...4) and their relative masonry panels (M1...4) without any surface preparation (A).

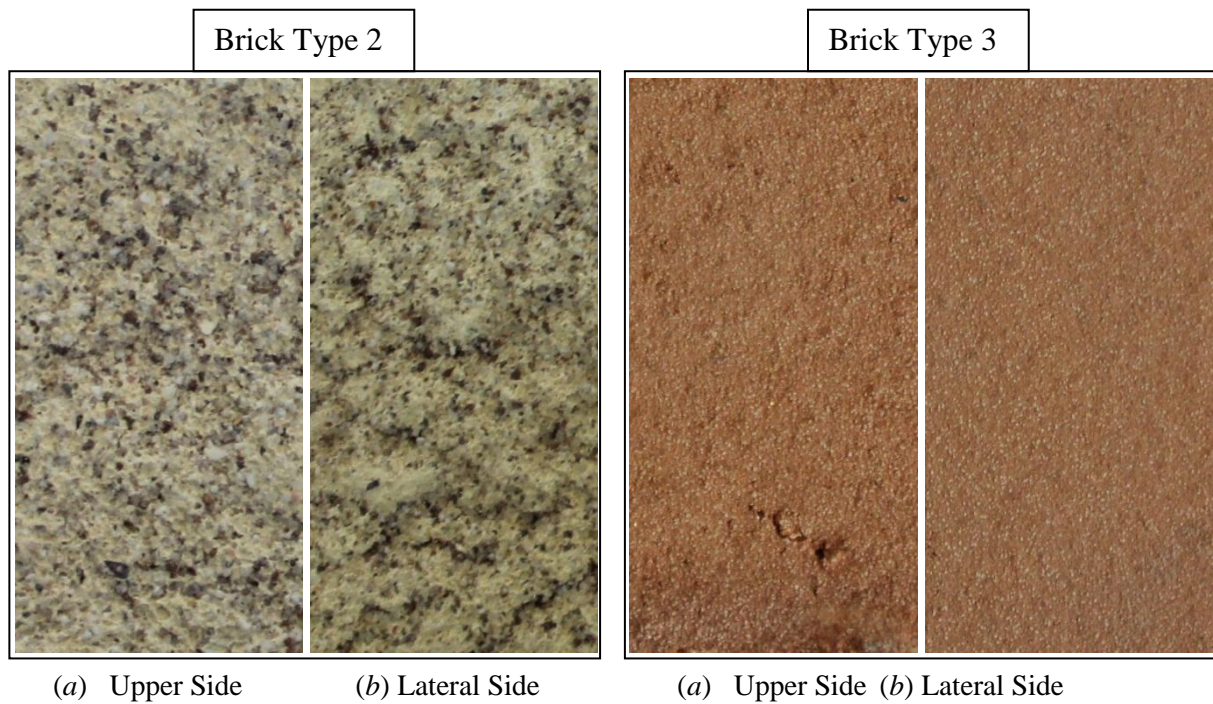


Figure 6: Surface of Brick Type 2 – 3: (a) Upper side used to glue FRP in tests on single brick B (b) lateral side used to glue FRP in tests on masonry elements M.

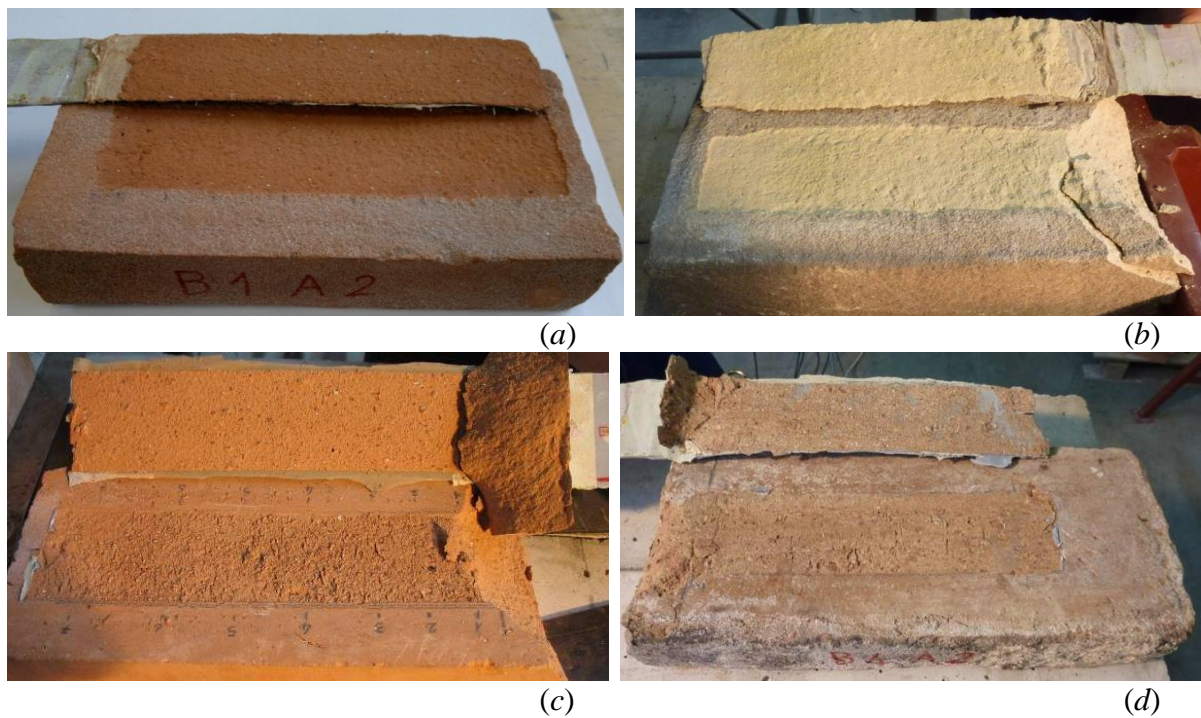


Figure 7. Debonding Failure Modes for GFRP-clay bricks: (a) B1A2, (b) B2A1, (c) B3A2, (d) B4A2.



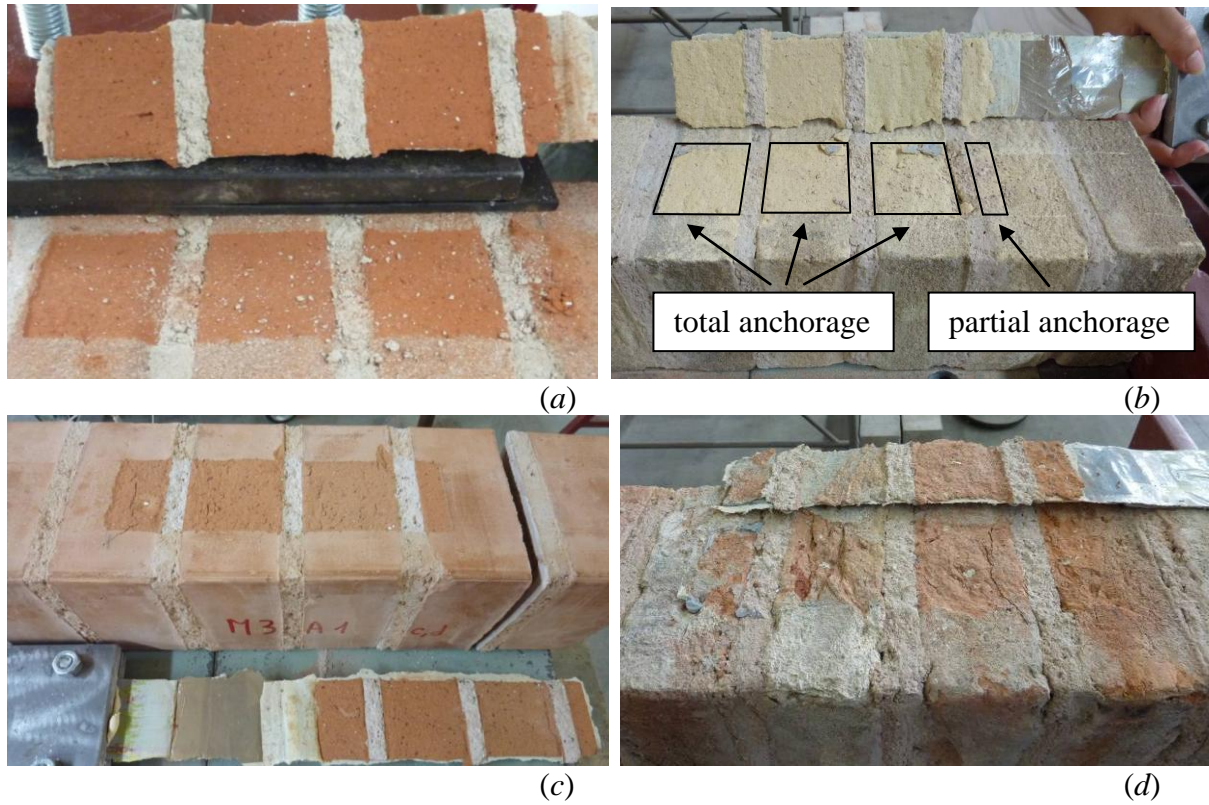
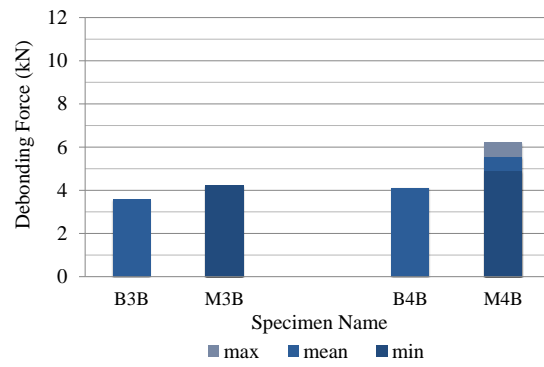
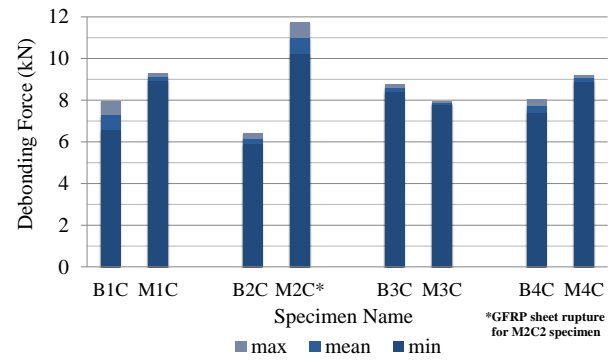


Figure 8. Bond failure modes for GFRP-masonry panels: (a) M1A1, (b) M2A1, (c) M3A1, (d) M4A1.



(a)



(b)

Figure 9. Maximum, minimum and mean values of debonding force obtained by different clay bricks (B) and their relative masonry panels (M) prepared applying: (a) a mortar based on natural hydraulic lime on the surface (finishing B), (b) a two-component polymer modified cementitious mortar on the surface (finishing C).





(a)



(b)

Figure 10. Debonding Failure Modes for: (a) B3B1, (b) M3B1.

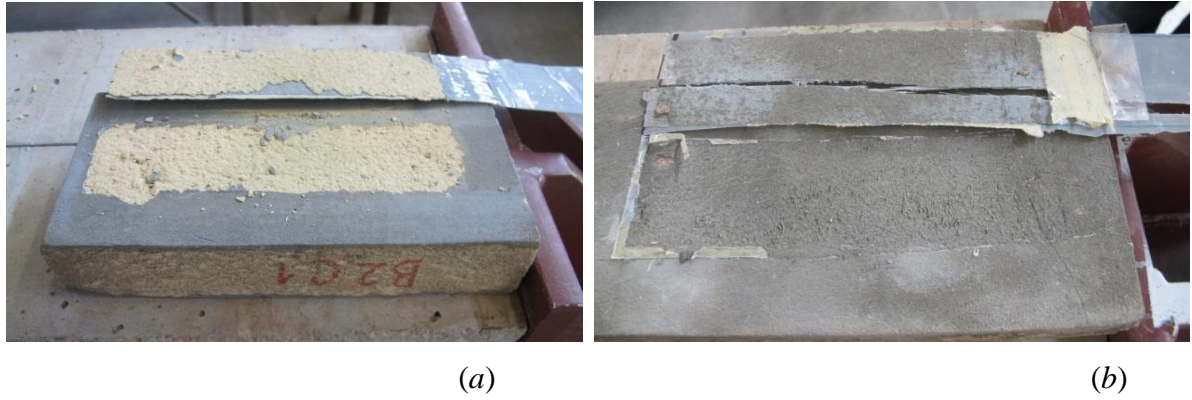


Figure 11. Debonding Failure Modes for GFRP-clay bricks: (a) B2C1, (b)B4C2.

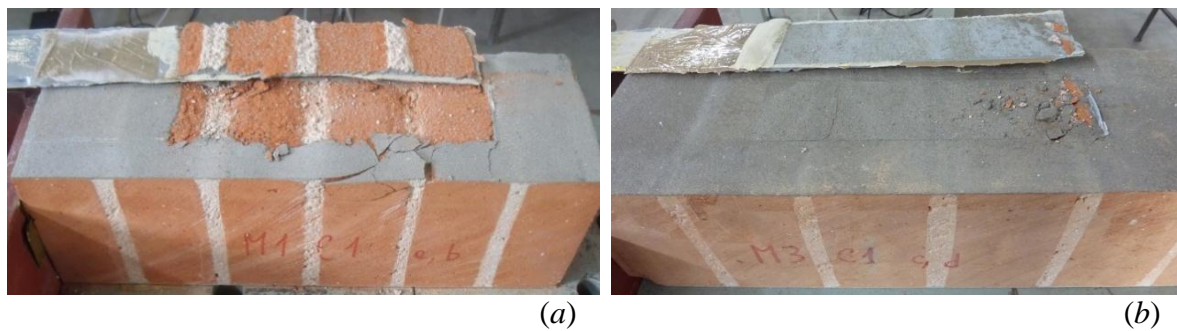


Figure 12. Bond failure modes for GFRP-masonry panels: (a) M1C1, (b) M3C2 .

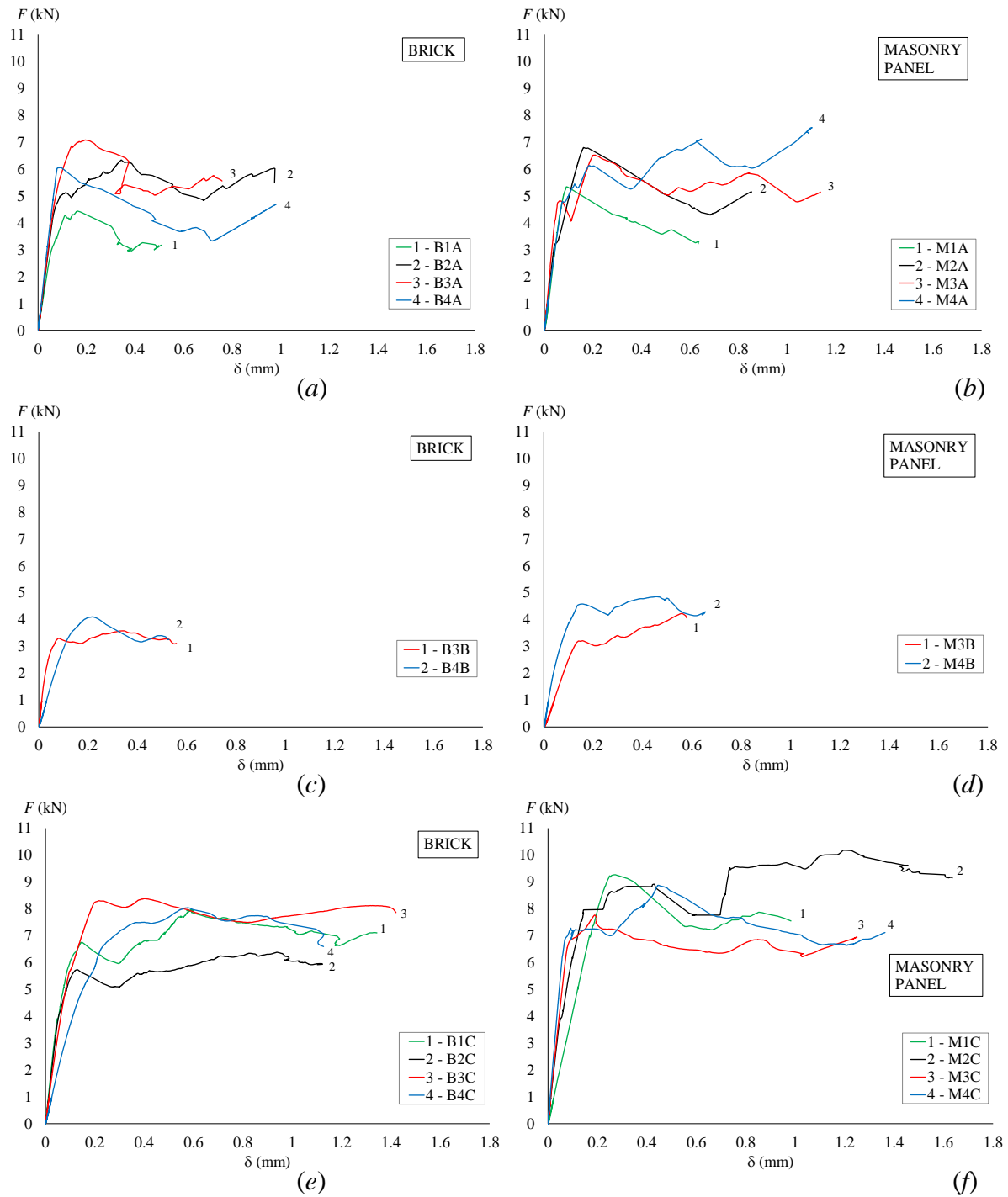


Figure 13. Load-slip curves: (a) brick specimens without surface preparation; (b) masonry panels without surface preparation A; (c) brick specimens with B finishing; (d) masonry specimens with B finishing; (e) brick specimens with C finishing; (f) masonry panels with C finishing.

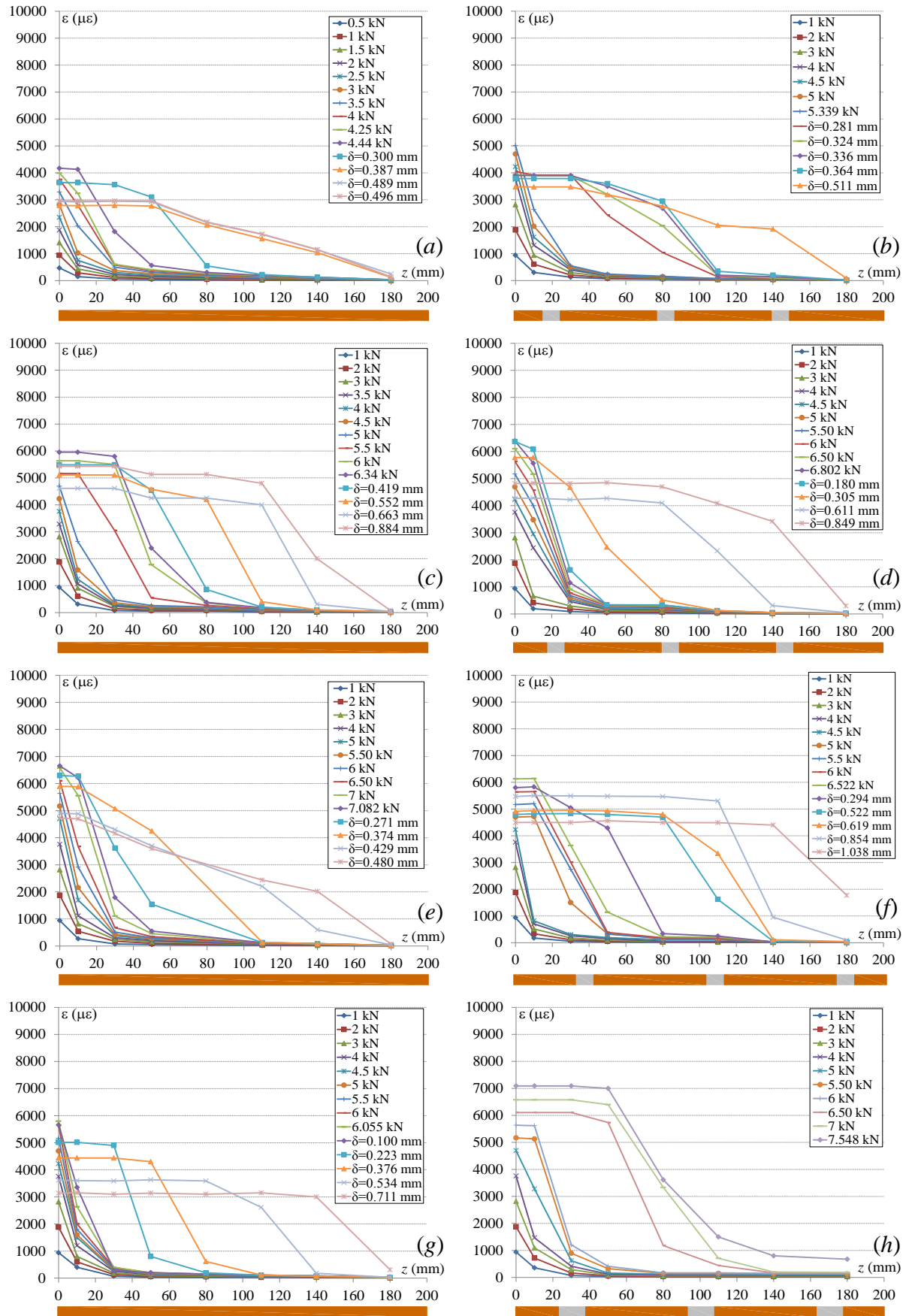


Figure 14. Strain along the specimens: (a) B1A; (b) M1A; (c) B2A; (d) M2A; (e) B3A; (f) M3A; (g) B4A; (h) M4A.

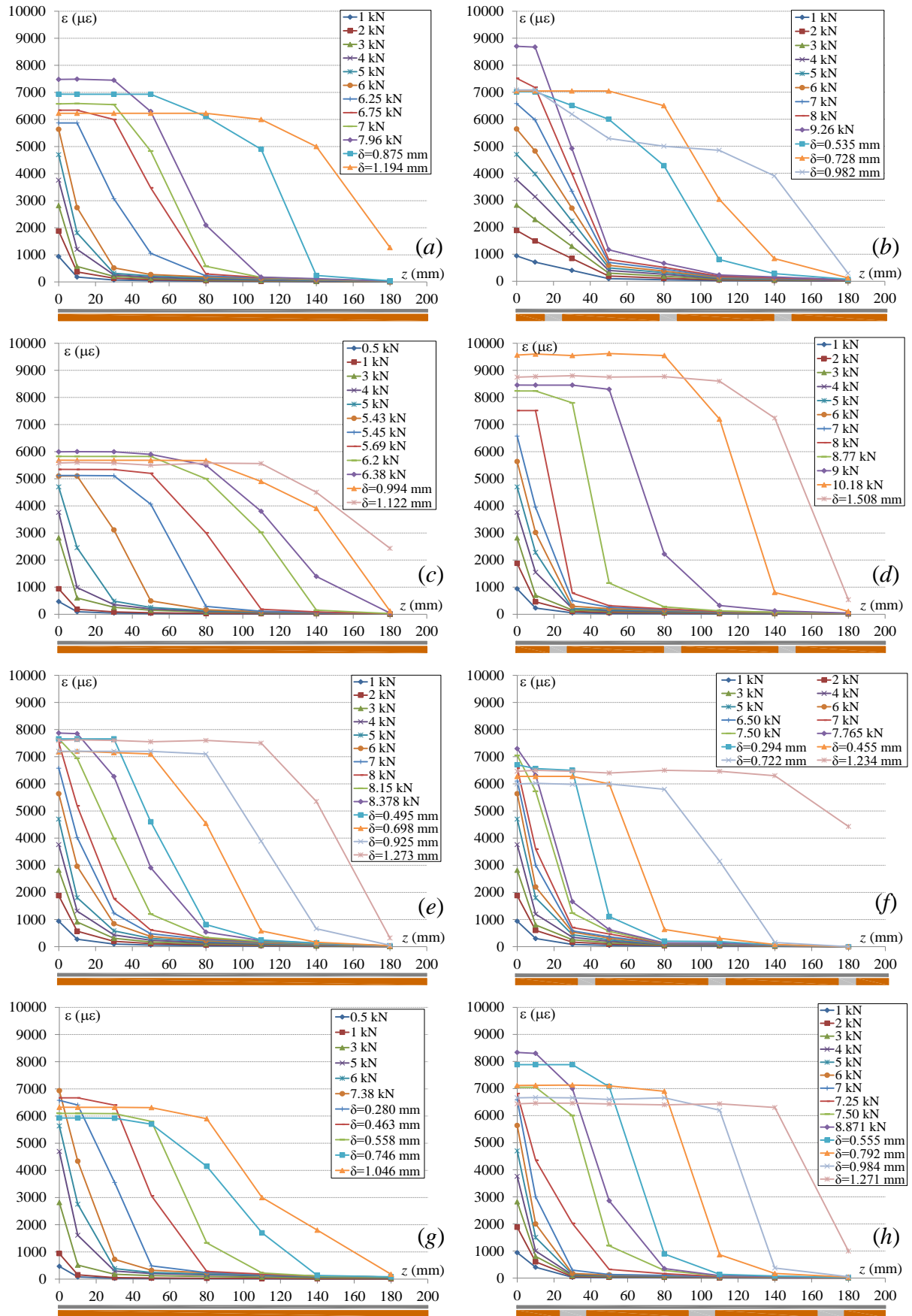
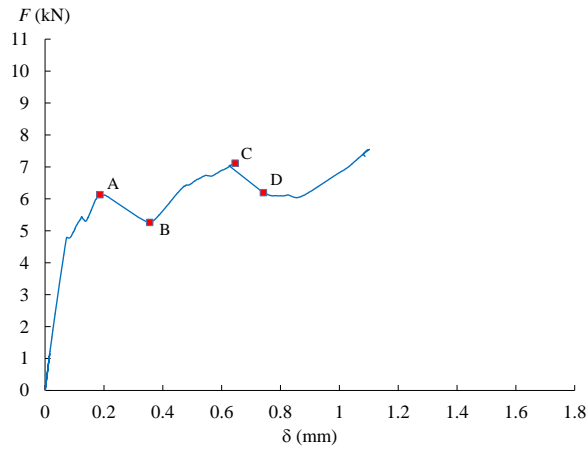
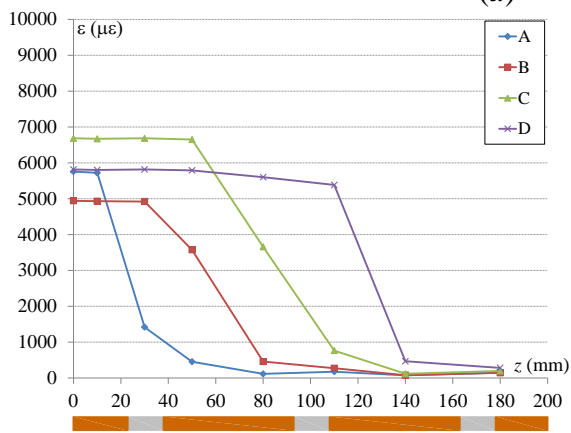


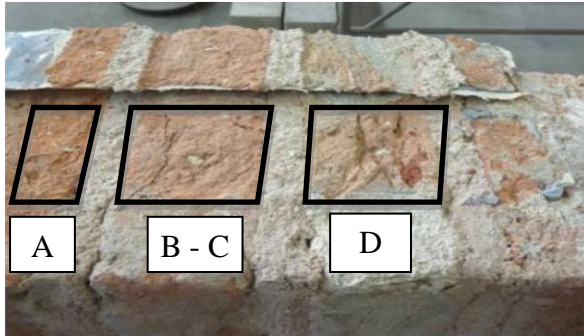
Figure 15. Strain along the specimens: (a) B1C; (b) M1C; (c) B2C; (d) M2C; (e) B3C; (f) M3C; (g) B4C; (h) M4C.



(a)



(b)



(c)

Figure 16. M4A: (a) Load-slip curve; (b) Strain along the specimens; (c) Failure mode.



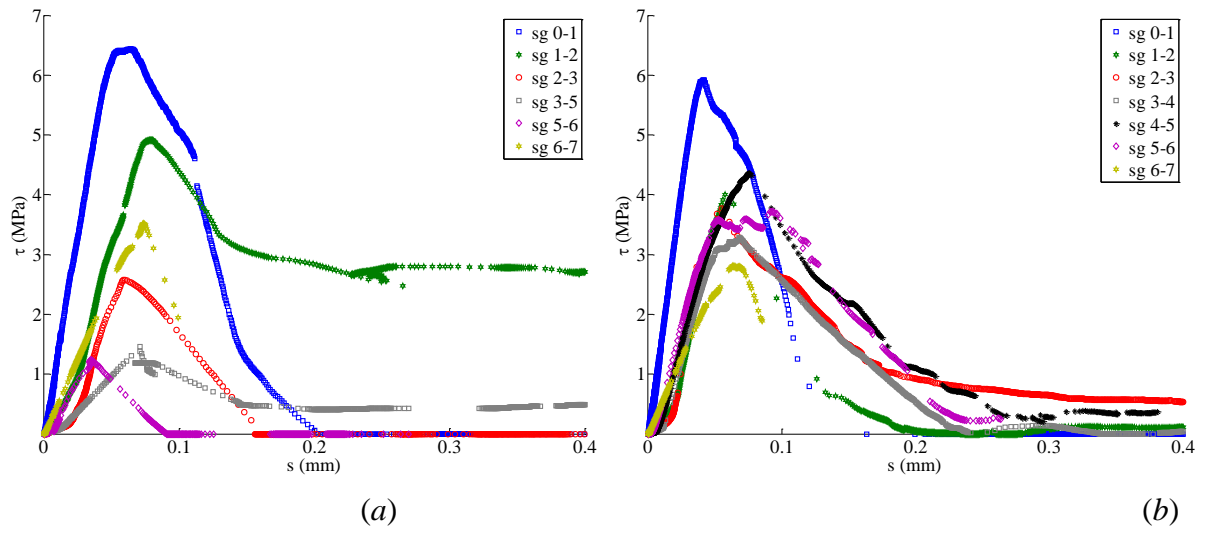


Figure 17. Shear stress versus slip: (a) B3A, (b) B2C.



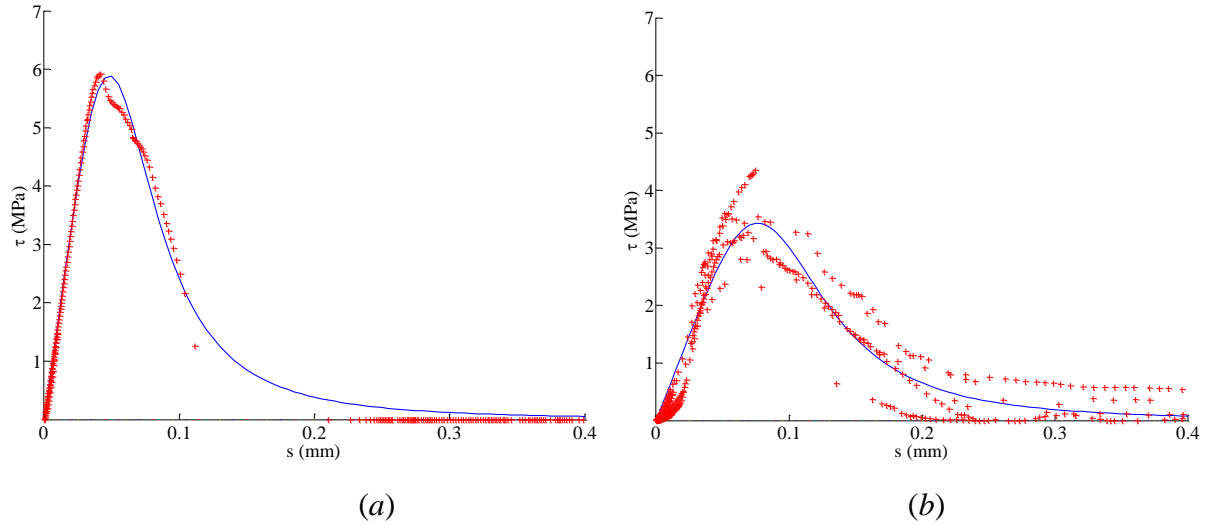


Figure 18. B2C specimen: postprocessing data and local shear stress - slip curve: (a) for the first part of the anchorage length est 0-1;(b) for the rest part of the anchorage length.